GCM Simulations of the Aerosol Indirect Effect: Sensitivity to Cloud Parameterization and Aerosol Burden

Surabi Menon

NASA Goddard Institute for Space Studies, and Center for Climate Systems Research, Columbia University, New York, New York

Anthony D. Del Genio

NASA Goddard Institute for Space Studies, New York, New York

Dorothy Koch

NASA Goddard Institute for Space Studies, and Center for Climate Systems Research, Columbia University, New York, New York

George Tselioudis

NASA Goddard Institute for Space Studies, and Department of Applied Physics, Columbia University, New York, New York

ABSTRACT

In this paper the coupling of the Goddard Institute for Space Studies (GISS) general circulation model (GCM) to an online sulfur chemistry model and source models for organic matter and sea salt that is used to estimate the aerosol indirect effect is described. The cloud droplet number concentration is diagnosed empirically from field experiment datasets over land and ocean that observe droplet number and all three aerosol types simultaneously; corrections are made for implied variations in cloud turbulence levels. The resulting cloud droplet number is used to calculate variations in droplet effective radius, which in turn allows one to predict aerosol effects on cloud optical thickness and microphysical process rates. The aerosol indirect effect is calculated by differencing the top-of-the-atmosphere net cloud radiative forcing for simulations with present-day versus pre-industrial emissions. Both the first and second indirect effects are explored. The sensitivity of the results presented here to cloud parameterization assumptions that control the vertical distribution of cloud occurrence, the autoconversion rate, and the aerosol scavenging rate, each of which feeds back significantly on the model aerosol burden, are tested. The global mean aerosol indirect effect for all three aerosol types ranges from -1.55 to -4.36 W m^{-2} in the simulations. The results are quite sensitive to the preindustrial background aerosol burden, with low preindustrial burdens giving strong indirect effects, and to a lesser extent to the anthropogenic aerosol burden, with large burdens giving somewhat larger indirect effects. Because of this dependence on the background aerosol, model diagnostics such as albedo-particle size correlations and column cloud susceptibility, for which satellite validation products are available, are not good predictors of the resulting indirect effect.

1. Introduction

The greatest uncertainty in the assessment of climate forcing by anthropogenic aerosols is their effect on clouds, referred to as the aerosol indirect effect (AIE). For a given cloud liquid water content (LWC), an increase in the cloud droplet number concentration (N) implies a decrease in the effective radius (r_{eff}), thus increasing the cloud reflectivity (Twomey 1977); this is known as the first indirect effect. Several studies have attempted to observe the Twomey effect in clouds mod-

ified by ship tracks (Coakley et al. 1987; Radke et al. 1989; King et al. 1993; Coakley et al. 2000; Durkee et al. 2000) or continental sources of pollution (Saxena and Menon 1999; Brenguier et al. 2000). The second indirect effect is based on the idea that decreasing the mean droplet size in the presence of enhanced aerosols decreases the cloud precipitation efficiency, producing clouds with a larger LWC and longer lifetime (Albrecht 1989; Pincus and Baker 1994). Recent results from the Monterey Area Ship Track (MAST) experiment (Ferek et al. 2000) and Tropical Rainfall Measuring Mission (Rosenfeld 2000) provide anecdotal evidence that anthropogenically forced decreases in r_{eff} can significantly alter the liquid water path (LWP) and suppress rainfall. Observations of aerosol-induced changes in cloud lifetime have not been reported, however.

Corresponding author address: Dr. Surabi Menon, Columbia University/NASA Goddard Institute for Space Studies, 2880 Broadway, New York, NY 10025.
E-mail: smenon@giss.nasa.gov

Observational assessment of both indirect effects is problematic because (a) direct measurements of aerosols and cloud properties are localized in space and time and cannot be used to infer global radiative impacts, and (b) it is difficult to isolate the aerosol effect on clouds from the natural variability in r_{eff} and LWC caused by changes in the cloud thermodynamical structure and the dynamics. Satellite datasets have begun to provide some cloud-top or vertically integrated measures of relevant cloud properties (Han et al. 1994, 1998a,b, 2000; Kaufman and Fraser 1997), but by themselves do not give a measure of the radiative impact of aerosols on clouds. Furthermore, global climatologies of aerosol properties exist only over ocean, provide only the column optical thickness, do not differentiate among aerosol types, and have large uncertainties due to contamination by thin clouds (Stowe et al. 1997). Thus, the only way to estimate the global AIE is by combining model simulations with satellite observational constraints (cf. Boucher 1995; Kogan et al. 1997). Unfortunately, existing general circulation model (GCM) simulations of the AIE span an unacceptably broad range, from near 0 to -5 W m^{-2} (Jones et al. 1994; Boucher and Lohmann 1995; Chuang et al. 1997; Lohmann and Feichter 1997; Rotstayn 1999; Kiehl et al. 2000; Ghan et al. 2001a). No observational constraints have been demonstrated to limit this range. To date, all that can be said is that the larger AIE predictions are less likely to be correct in light of the observed global temperature increase that has accompanied an accumulated anthropogenic greenhouse gas forcing of only 2.5 W m^{-2} (Hansen et al. 2000).

Most previous GCM research on the AIE has emphasized the uncertainties associated with determining the aerosol distribution and its effect on cloud properties. GCMs take two different approaches to determine N. Some models predict N from aerosol chemical and microphysical properties by means of a sophisticated aerosol nucleation and growth model (Chuang et al. 1997; Lohmann et al. 1999; Ghan et al. 2001a,b), thereby making it possible for N to be a prognostic variable. This has the appeal of being physically based, but it requires underlying assumptions about (a) the unresolved small-scale turbulent updraft velocity, a quantity that is especially difficult to predict within clouds, and (b) the efficiency with which different aerosol types nucleate cloud droplets, which depends on details of the aerosol composition and the unknown extent of internal versus external mixing. Other models use a simple empirical diagnostic approach, directly parameterizing N as a function of either aerosol mass or aerosol number concentration based on field observations (Jones et al. 1994; Lohmann and Feichter 1997; Rotstayn 1999; Kiehl et al. 2000). This bypasses the difficult physics of cloud droplet formation, and by using sulfate as a proxy for all aerosols, the diagnostic approach in principle allows for the indirect effect of all aerosols in a model that only explicitly simulates the sulfate distri-

bution. The disadvantage of the diagnostic approach is that it is based on limited information from local or regional field studies that sample a specific mix of aerosol types in specific meteorological conditions, which compromises their usefulness in global applications. Some models determine N diagnostically using monthly mean sulfate fields computed offline; in such models the aerosol affects the cloud but the cloud is not allowed to feed back on the aerosol distribution.

In both approaches a major additional uncertainty concerns natural sources of aerosols or their precursors. In this regard, evaluation of the AIE is much more difficult than for climate forcing due to greenhouse gas emissions. For greenhouse gas forcing the preindustrial concentration levels are well known, and anthropogenic increases thus far have not yet even doubled the effective background concentration. For aerosols, on the other hand, there is probably no vegetated continental location anywhere that retains a pristine environment, and thus there is no way to reliably determine the preindustrial continental background aerosol level. Over oceans, the natural sulfate contribution from dimethyl sulfide (DMS) emissions is still uncertain (Charlson et al. 1987; Kettle and Andreae 2000) and the role of sea salt depends in a complex fashion on meteorological conditions and the coincident presence of sulfate (Ghan et al. 1998; O'Dowd et al. 1999). Furthermore, anthropogenic aerosol increases to date dwarf the background levels near and downwind of pollution sources. Thus, considering that the susceptibility of clouds is greatest in relatively clean conditions (Platnick and Twomey 1994), the uncertainty in the background aerosol concentration itself introduces significant variability in the simulated present-day AIE (Chuang et al. 1997; Kiehl et al. 2000).

By comparison, much less attention has been paid to the effect of cloud parameterization assumptions on the simulated AIE. Lohmann and Feichter (1997), Rotstayn (1999), and Ghan et al. (2001b) have explored the sensitivity of the second indirect effect to different autoconversion and cloud-cover parameterizations. Different autoconversion schemes have markedly different dependence of rain formation on N and LWC, and are intended for use on the cloud scale, rather than the GCM grid scale; but subgrid variability can potentially have a great impact on microphysical process rates (Pincus and Klein 2000; Rotstayn 2000). Cloud formation schemes in GCMs are not yet either physically based or even empirical (because subgrid-scale vertical velocity effects on cloud formation are usually not represented), so the effect of initial cloud formation assumptions on the AIE can potentially vary widely. Mace et al. (1998) highlight the possibility of using cloud radar from polar orbiting satellites for global scale model vertical cloud-distribution comparison. However, to date, little attention has been paid to the ability of GCMs to simulate the detailed vertical distribution of cloudiness in the lower troposphere, despite the fact that the

aerosol concentration decreases sharply above the surface and the AIE depends on the colocation of aerosol and cloud. Coakley et al. (2000) found that the presence or absence of ship tracks in MAST data was quite sensitive to the relative heights of the aerosol layer and the cloud top, suggesting that these details might be important for simulation of the AIE. The feedback of cloud processes on the aerosol distribution, for example, via the in-cloud oxidation source and wet deposition sink, has been mostly ignored, although Lohmann and Feichter (1997) comment on the effect of different cloud formation parameterizations on the resulting aerosol field.

In this paper we describe initial results from a version of the Goddard Institute for Space Studies (GISS) GCM that has been coupled to an aerosol source–chemistry model, with particular emphasis on how model cloud-parameterization assumptions influence the simulated AIE and how existing observations do or do not constrain AIE estimates. The basic coupled model structure and design of sensitivity experiments are described in sections 2 and 3, respectively. Resulting distributions of the aerosol concentration and the AIE for the different simulations are described in section 4. In section 5 we evaluate our results against various satellite diagnostic quantities. We discuss the implications of our work and possible future directions of research in section 6.

2. Model description

a. General circulation model

We use the GISS Model II GCM (Hansen et al. 1997), a gridpoint model with $4° \times 5°$ horizontal resolution and nine vertical sigma coordinate levels and a dynamical top at 10 mb. This GCM was developed from the GISS GCM Model II (Hansen et al. 1983), with several improvements: notably a new prognostic cloud water scheme for stratiform clouds (Del Genio et al. 1996), improved mass flux cumulus parameterization (Del Genio and Yao 1993), a second-order closure planetary boundary layer, and improved ground hydrology (Rosenzweig and Abramopoulos 1997). Stratiform cloud generation is relative humidity (RH) dependent, based on the approach of Sundqvist et al. (1989), but also includes a dependence on moist stability. Clouds form when RH exceeds a threshold that is specified for all model levels except for the lowest layer. In the lowest layer the threshold RH is calculated as the RH for which a parcel would saturate if lifted from the bottom to the top of the layer. The GCM allows for fractional cloudiness in the vertical as well as horizontal, that is, a cloud physical thickness that is less than the GCM layer thickness, depending on stability. Microphysical sinks for liquid water include autoconversion, evaporation, cloud-top entrainment, accretion, and the Bergeron–Findeisen process. All clouds form as liquid for temperatures $>-4°C$ over oceans and $-10°C$ over land, and as ice for temperatures $<-40°C$. In between these temperatures, a probability function is used for formation of ice (Del Genio et al. 1996). A fixed value of N (0.06 cm^{-3}) is used for all ice clouds. The cumulus parameterization uses a cloud base neutral buoyancy mass flux closure and includes convective downdrafts, entraining and nonentraining plumes, detrainment of condensate into anvils, and evaporation of precipitation. The radiation scheme includes all important radiatively active species; it uses the correlated k-distribution approach for gaseous absorption and a single Gauss point adaptation of the doubling and adding method for multiple scattering.

b. Aerosol model

We simulate the indirect effects associated with sulfate, organic carbon, and sea-salt aerosols. Aerosol distributions are calculated online and are fully interactive with the GCM dynamics and physics. Details of included aerosols are listed below and are summarized in Table 1.

1) SULFATE

The sulfate chemistry model (Koch et al. 1999) includes SO_2, sulfate, dimethylsulfide (DMS), and H_2O_2 as prognostic species. It uses a resistance in series dry deposition scheme and has a wet deposition and in-cloud chemistry scheme that is coupled to the GCM cloud schemes. For large-scale clouds, the autoconversion rates and the grid-box cloud fraction are used to calculate the first-order loss for precipitation scavenging. For moist convective clouds, all the dissolved tracers (in the updraft) are removed with the rainwater except for those that are evaporated or detrained. Below-cloud scavenging and evaporation of gases are also included. A detailed comparison of the simulated sulfate distribution with observations is presented in Koch et al. (1999).

TABLE 1. Chemical species and sources for sulfate, OM, and sea salt aerosols. ANTH and NATL refer to anthropogenic and natural aerosol sources, respectively.

Species	Sources	References
ANTH sulfate	Seasonally varying GEIA SO_2 emissions	Benkovitz et al. 1996
	Aircraft source	Baughcum et al. 1993
	Biomass burning	Spiro et al. 1992
NATL sulfate	DMS oceanic source	Kettle et al. 1999; Liss and Merlivat 1986
	Noneruptive volcanic sources	Spiro et al. 1992
ANTH OM	Fossil fuel and biomass burning	Liousse et al. 1996; Cooke et al. 1999; Penner et al. 1993
NATL OM	Terpene emissions	Guenther et al. 1995
Sea salt	Ocean	Gong et al. 1997a

2) ORGANIC CARBON

The carbonaceous aerosol model of Koch (2001, manuscript submitted to *J. Geophys. Res.*, hereafter K01) includes both absorptive black carbon and the more refractive and more soluble organic carbon (OC; we consider only the latter here). The OC emissions for biomass burning and industry are from Liousse et al. (1996). As in Liousse et al. (1996), we use the organic matter (OM), where OM = 1.3 × OC to account for the presence of noncarbon elements. The emissions for OC are highly uncertain and measurements available for model validation are extremely sparse, with few datasets spanning a full year. K01 found the total model bias against observations to be low; however, the scatter was high, with the model typically within a factor of 10 of observations. The source for natural OM emissions from terpenes is from Guenther et al. (1995). A 10% yield rate of OM from terpenes is assumed, which is higher than that used in Liousse et al. (1996) but at the low end of that in Andreae and Crutzen (1997).

3) SEA SALT

Sea-salt concentrations in six size bins are from Gong et al. (1997a) who used the Monahan et al. (1986) source and the National Center for Atmospheric Research Climate System Model to treat sea-salt dependence on wind speed. In this study, we input monthly sea-salt concentrations from the first four bins (sizes 0.03–0.25 μm, 0.25–0.50 μm, 0.50–1.0 μm, and 1.0–2.0 μm), since modeling (Ghan et al. 1998) and observational studies (O'Dowd et al. 1999) indicate that film and jet modes are most important (in terms of sea-salt number and surface area concentrations, respectively) in modifying the sulfate distribution. Sea salt is assumed to be fully soluble for wet deposition purposes. In addition to removal by wet and (resistance-in-series) dry deposition, gravitation settling is included.

c. Aerosol direct effect

Although the direct aerosol radiative effect is treated, we restrict our discussion to the AIE since Koch et al. (1999) and K01 discuss the direct effect. The 0.55-μm aerosol optical thickness is obtained from the product of the aerosol mass and the specific extinction cross section as in Charlson et al. (1984) and aerosol interaction with radiation is treated via Mie scattering theory. The effect of relative humidity on optical thickness is only applied for sulfate aerosols. At present, the water uptake rate for sea salt and organic carbon aerosols are not treated because of the uncertainty in the uptake rate. Instead we use a specific extinction that is applicable for an average relative humidity (K01), but would probably lead to an underestimation of optical thickness at high relative humidities (>90%; A. Lacis 2001, private communication).

d. Aerosol–cloud interaction

We use a simple diagnostic approach to calculate N from aerosol mass based on field observations. However, we attempt to partly address the limitations of this approach by developing multiple regressions against all three simulated aerosol types (rather than assuming sulfate to be a universal proxy) and by including an empirical correction factor that mimics the effect of varying cloud turbulence strength on N.

Field data from Leaitch et al. (1996) in the Northeast Atlantic, and from Borys et al. (1998) in Tenerife, were used to develop a multiple regression relationship between N, sulfate, OM, and sea salt. Since OM measurements were not reported in Borys et al., we parameterize OM as a function of sulfate using data from Tenerife obtained during the Second Aerosol Characterization Experiment (Putaud et al. 2000). This assumption is based on field measurements (Liu et al. 1996; Matsumoto et al. 1997; Putaud et al. 2000) that indicate a positive correlation between sulfate and OM. Since the data were obtained from the same location at similar times of the year, albeit from different experiments, variability in the ratio of OM to sulfate should not be an important factor. The Leaitch et al. dataset did not have complete measurements of all species of OM and therefore could underestimate the actual OM for the Northeast Atlantic (W. R. Leaitch 2000, personal communication). Identical regressions are applied over land and ocean, except that sea salt is included only in the latter. The resulting multiple regression relationships to predict N for land, N_{Land}, and ocean, N_{Ocean}, are

$$N_{\mathrm{Land}} = 10^{\{2.41+0.50\,\log(\mathrm{Sulfate})+0.13\,\log(\mathrm{OM})\}}, \quad \text{and} \qquad (1a)$$

$$N_{\mathrm{Ocean}} = 10^{\{2.41+0.50\,\log(\mathrm{Sulfate})+0.13\,\log(\mathrm{OM})+0.05\,\log(\mathrm{Sea\text{-}salt})\}}, \qquad (1b)$$

where sulfate, OM, and sea salt are the mass concentrations in μg m^{-3} and N is in cm^{-3}; N predicted using the above equations is more sensitive to changes in sulfate than to OM due to the higher slope for sulfates, however, the AIE has not been evaluated separately for either sulfates or OM alone. These regressions differ from the commonly used empirical relationships given in Boucher and Lohmann (1995) in their modeling study on the AIE. Their relationships were based on simultaneously measured sulfate and either cloud condensation nuclei (CCN) or N. When only CCN data were available, they assumed that the measured CCN concentration used was the same as N in deriving their N–sulfate relationships. This assumption is not true, as under varying supersaturations, updraft speeds, etc., the empirical relationship between CCN and N is nonlinear (Menon and Saxena 1998; Snider and Brenguier 2000). The advantage of relating N with aerosol mass, as given in (1a) and (1b), is that these implicitly take into account the physics (updraft velocity, size spectra, growth rate, supersaturation profiles, etc.) that actually determines N, while explicitly representing the contribution of the three different aerosol species, allows us to more con-

TABLE 2. Designation of experiments used for model simulations of the AIE. Also included is the length of model runs. The different columns indicate the sensitivity tests conducted to evaluate the AIE. D96 refers to Del Genio et al. (1996), TC80 to Tripoli and Cotton (1980), and K99 to Koch et al. (1999).

Experiment	Number of years averaged	AIE	Cloud vertical distribution	Autoconversion	Scavenging
CTRL-R	5	1st	f (layer 1 thickness)	D96	K99
NEWCLD-R	5	1st	$f(\mathrm{Ri})$	D96	K99
NEWCLD-M-7.5	2	1st and 2nd	$f(\mathrm{Ri})$	TC80 (r_{crit}=7.5 μm)	K99
NEWCLD-M-5.0	2	1st and 2nd	$f(\mathrm{Ri})$	TC80 (r_{crit}=5.0 μm)	K99
NEWCLD-M-5.0-P	5	1st and 2nd	$f(\mathrm{Ri})$	TC80 (r_{crit}=5.0 μm)	Decreased scavenging

fidently apply the regression to other regions with different mixes of aerosol types.

Leaitch et al. (1996) have highlighted the role of turbulence in modifying N for a given aerosol concentration. Higher updraft speeds increase the activation of aerosol particles, which thus increases N. Under stable conditions, N is reduced because the lower updraft speeds produce supersaturations that are not high enough to activate smaller size particles. We use the GCM's parameterization of cloud top entrainment (CTE) as an indicator of within-cloud turbulence. The parameterized CTE mixing depends on the moist static energy jump across the cloud-top interface and on the total water content in the cloud (Del Genio et al. 1996). To mimic the Leaitch et al. observations, we scale N as predicted by (1a) and (1b) by a factor that ranges from 1.5 in high CTE (unstable, strong turbulence) conditions to 0.5 in zero CTE (extremely stable, weak turbulence) conditions.

Given N, the volume-weighted mean cloud droplet radius r_{vol} is determined by, $r_{\mathrm{vol}} = [(3\mathrm{LWC})/(4\pi\rho_1 N)]^{1/3}$, where ρ_1 is liquid water density. This value is applied to determine aerosol effects on cloud microphysical processes (autoconversion, cloud evaporation). The r_{eff} needed to compute cloud radiative properties is obtained from r_{vol} assuming a standard gamma size distribution with an effective variance of 0.2 given as $r_{\mathrm{eff}} = 1.28$ r_{vol}. Cloud optical depth (τ) is then evaluated by, $\tau = (1.5 \, \mathrm{LWP})/(\rho_1 \, r_{\mathrm{eff}})$. For a given τ and r_{eff}, cloud radiative properties are computed using the spectral dependence predicted by Mie theory (Hansen and Travis 1974). Aerosols are only allowed to affect liquid-phase clouds, so the longwave contribution to AIE is small in all the experiments.

3. Experimental setup

The AIE is defined as the difference in the net cloud radiative forcing between simulations that use present-day (PD; natural plus anthropogenic) aerosols and simulations that use preindustrial (PI; natural) aerosols. Baseline model runs are forced by climatological sea surface temperature fields for the period 1978–98 and are carried out for 6 yr, with the results based on the final 5-yr averages. For sensitivity studies, shorter model runs for 3 yr (with results based on 2-yr averages) are

carried out. We examine five (PD, PI) pairs of simulations (Table 2), defined in sections 3a–e.

a. CTRL-R

This run uses the standard model configuration described in the previous section and accounts only for the first indirect effect. In this run, the autoconversion rate (Q) is an increasing function of the cloud LWC with no dependence on N except for specified land–ocean differences in efficiency (Del Genio et al. 1996).

b. NEWCLD-R

In common with most GCMs, the GISS model tends to overpredict cloudiness in the lowest model layer. For most applications this is not a serious defect, but given the sharp decrease in aerosol concentration away from the surface, even small errors in cloud altitude can influence the simulated AIE. The frequency of occurrence of low-level cloud tops in GCM layers 1, 2, and 3 (top pressure = 934, 854, and 720 hPa, respectively) in CTRL-R is 36%, 30%, and 34%, respectively. Data from the International Satellite Cloud Climatology Project (ISCCP) mapped to the GCM layers indicate an occurrence distribution of 16%, 26%, and 58%, respectively, instead.

We therefore modified our calculation of the threshold RH for cloud fraction as follows: In the standard scheme described earlier, the threshold RH for the lowest layer is based on implied lifting over the layer depth, which is only appropriate if the lowest layer is dry convective with respect to layer 2, that is, if there are subgrid vertical motions that extend over a full layer. In NEWCLD-R, the full layer thickness is used to calculate the threshold RH only if layer 1 is unstable with respect to the next higher layer. In all other cases, the implied subgrid lifting only goes from the bottom of the layer to a height Z determined by the degree of stability, as follows: if the Richardson number between layer 1 and layer 2 (Ri_{12}) ≤ 1 (an approximate upper limit for small-scale turbulence in the model of Cheng et al. 2002), then

$$Ri_{12} < 0.25 \Rightarrow Z = \text{top height of layer 1 } (Z_1),$$

$$0.25 \leq Ri_{12} < 1 \Rightarrow Z = \text{interpolated height between } Z_1 \text{ and midpoint of layer 1 } (Z_m), \quad \text{and}$$

$$Ri_{12} = 1 \Rightarrow Z = Z_m,$$

If $Ri_{12} > 1$, a similar calculation is performed for Ri between the surface air layer and layer 1 (Ri_{s1}), such that

$$Ri_{s1} < 0.25 \Rightarrow Z = Z_m,$$

$$0.25 \leq Ri_{s1} < 1 \Rightarrow Z = \text{interpolated height between } Z_m \text{ and the surface layer height } (Z_0), \quad \text{and}$$

$$Ri_{s1} \geq 1 \Rightarrow Z = Z_0.$$

The prescribed threshold RH for all higher layers is decreased (set at 0.57) at the same time so as to produce a total cloud cover and planetary albedo roughly equivalent to those in CTRL-R. The net effect of the parameterization change is to reduce cloudiness in layer 1 under more stable PBL conditions and to increase cloudiness in higher layers. The resulting cloud-top distribution in NEWCLD-R is 26%, 43%, and 31%, respectively, in better agreement with the ISCCP data. The remaining model-data discrepancy is at least in part an ISCCP bias caused by inaccuracies in its input humidity profiles, which cause it to overpredict cloud height by 60–80 hPa in marine stratus regions (Wang et al. 1999).

c. NEWCLD-M-7.5

This scheme differs from NEWCLD-R only in that it allows for the second as well as the first indirect effect. To evaluate the second indirect effect, an autoconversion parameterization from Tripoli and Cotton (1980; hereafter referred to as TC) is implemented. Here, autoconversion does not occur unless the in-cloud liquid water mixing ratio q_1 exceeds a certain critical limit q_{crit} defined as

$$q_{crit} = (4\pi\rho_1 r_{crit}^3 N)/(3\rho), \tag{2}$$

where r_{crit} is the critical value of the droplet radius that would initiate precipitation and ρ is the air density. The autoconversion rate is then given by

$$Q = \frac{0.104 g E_{AU} \rho^{4/3}(q_1)^{7/3} H(q_1 - q_{crit})}{\varepsilon(N\rho_1)^{1/3}}, \tag{3}$$

where H is the Heaviside function, E_{AU} is the droplet collection efficiency set to 0.55, g is the acceleration due to gravity, and ε is the dynamic viscosity of air. High values of N increase the threshold limit and also decrease Q. Low values of r_{crit} result in increased precipitation and thus a smaller indirect effect. Values generally used in different climate models vary from 4.5 to 10 μm (Rotstayn 1999; Boucher et al. 1995; Rasch

and Kristjansson 1998). In NEWCLD-M-7.5 we assume $r_{crit} = 7.5 \ \mu$m.

d. NEWCLD-M-5.0

This experiment is identical to NEWCLD-M-7.5 but with $r_{crit} = 5.0 \ \mu$m, which enhances the autoconversion rate and thus reduces the importance of the second indirect effect.

e. NEWCLD-M-5.0-P

The first-order rate-loss parameterization in the stratiform in-cloud scavenging scheme depends on the amount and areal coverage of precipitation in the cloudy part of the grid box. The baseline model assumes that the fraction of the grid box that is precipitating equals the product of the subgrid cloud areal fraction and the ratio of precipitating to total condensed water (Koch et al. 1999). Thus, in dense clouds, most of the cloud area precipitates and participates in scavenging below. This is probably an overestimate, based on the satellite analysis of Lin and Rossow (1997) who find that only ∼5% of pixels between 50°S and 50°N contain precipitation. In NEWCLD-M-5.0-P we assume that precipitation occurs in only 10% of the cloudy area. This reduces scavenging and thus increases aerosol concentration. This probably represents a lower limit for the role played by precipitation, but it serves as a useful sensitivity test for the resulting radiative impact of a process not generally associated with radiative issues.

4. Results

a. Aerosol mass distribution

The aerosol column burdens for the PD and PI aerosol sources for the five model runs are listed in Table 3. Detailed comparisons of sulfate and OM distribution with observations for a model version similar to CTRL-R can be found in Koch et al. (1999) and K01. Although the magnitudes of the column burden differ, all five simulations have similar horizontal distributions and vertical profiles. As one example, we show the present-day aerosol mass distributions in μg m^{-3} for sulfate, OM and sea salt for January and July for model layer 1 ($P = 959$ hPa) for the NEWCLD-M-5.0-P run in Fig. 1. Figure 2 is similar to Fig. 1 but shows the vertical distribution of the mass (10^6 kg for sulfate and OM, and 10^7 kg for sea salt). Sulfate concentrations are the highest during summer over the NH continents due to increased oxidant availability, whereas they are higher over the SH oceans in summer due to the higher natural burden in summer. The model, similar to other models with prognostic H_2O_2, has a somewhat higher SO_2 burden compared with models using fixed H_2O_2 due to depletion of the in-cloud oxidant in polluted regions. The natural DMS source for sulfate is low compared to

TABLE 3. Globally averaged annual aerosol column burden (mg m^{-2}) for sulfate, OM, and sea salt for PD and PI emissions. Also included is the difference (Δ) between the PD and PI simulations.

Experiment	Sulfate			OM			Sea salt		
	PD	PI	Δ	PD	PI	Δ	PD	PI	Δ
CTRL-R	3.75	0.96	2.79	1.90	0.23	1.67	7.64	7.56	0.08
NEWCLD-R	4.02	1.14	2.88	2.15	0.29	1.86	7.91	7.92	−0.01
NEWCLD-M-7.5	2.66	0.42	2.24	1.57	0.14	1.43	4.16	3.70	0.46
NEWCLD-M-5.0	1.11	0.30	0.81	0.90	0.12	0.77	3.53	3.59	−0.06
NEWCLD-M-5.0-P	5.03	1.05	3.98	2.46	0.27	2.19	9.36	9.02	0.34

observations (and other models) in remote regions. This is due in part to weaker than observed GCM winds, and to the use of a low sea-to-air transfer rate for DMS. Because of this, all the sulfur species over the remote oceans tend to be lower than observed. Koch et al. (1999) found the sulfate surface concentrations on land to agree well with observations; however, the sulfate concentrations in the free troposphere above continents may be somewhat excessive.

Concentrations of OM are greater than sulfate in the SH due to the larger biomass burning source. Mass concentrations for OM are higher than sulfate mass in the first layer, though the OM column burden is much lower. This is because OM has only a surface source, while sulfate is formed only after oxidation of the SO_2 precursor that is often transported to higher layers. Model OM concentrations are lower than observations in the Pacific and Arctic but not over the Atlantic (K01).

Sea-salt concentrations are higher over the high latitude oceans during the winter months due to the stronger wind speeds there. For sea salt, comparison is performed with respect to the sodium content (assuming sodium content to be 0.3061 that of sea salt). Observations and model simulations of sodium content for five locations listed in Gong et al. (1997b) for NEWCLD-M-5.0-P (which has the highest sea-salt concentration of all the experiments) are shown in Fig. 3. Model simulations are in fairly good agreement and do capture the seasonality in the distribution.

b. Evaluation of cloud droplet number concentration

Since our prediction of N depends on the concentrations of three aerosol species and varies with the implied cloud turbulence strength, it is instructive to compare the resulting N–sulfate relationship to field measurements with simultaneous N and sulfate observations. Data for the land points are from Northeast America (Leaitch et al. 1992), Southeast United States (Menon and Saxena 1998), and the United Kingdom (Roelofs et al. 1998). Those for the ocean points are Northeast Atlantic (Leaitch et al. 1996), Puerto Rico (Novakov et al. 1994), and Tenerife (Borys et al. 1998). Most measurements were taken during summer with two exceptions: the Novakov et al. (1994) dataset also included cases from March–April, and the Northeast American dataset included winter and fall measurements. Main

differences between winter–fall and summer measurements are stronger updrafts, higher cloud bases, and higher N during summer and lower median sulfate values for winter, due to the lower cloud bases and mixing heights, which could lead to higher surface concentrations (Leaitch et al. 1992). The N predicted from the NEWCLD-M-5.0-P model run, as a function of sulfate mass along with the observed N–sulfate relationships, are shown in Figs. 4 and 5 for the land and ocean locations, respectively. Hourly averaged model values of N and sulfate were sampled four times during the daytime in July for model grid points and layers closest to the observational areas and altitudes.

Model sulfate values are within the range of observations for Northeast America, the United Kingdom, and Puerto Rico but are higher than observed for the Southeast United States and the Northeast Atlantic. Model N and sulfate values are systematically underestimated over Tenerife. The underprediction of N is probably related to an underestimate of OM simulated by the model there as well, though the sensitivity to sulfate appears to be similar to observations. For Puerto Rico, observations are limited and the sensitivity of N to sulfate appears low (Novakov et al. 1994). Furthermore, the data suggest that OM dominates sulfate over this region, though the model prediction is the opposite. Differences in slopes between model and observations are within 15% for the combined land locations, but the model systematically overestimates the slope over ocean relative to the available data. The discrepancy is primarily due to our underprediction of N over Tenerife, and the NE Atlantic points, since our regression utilizes data from Leaitch et al. for this location that do not measure all species of OM. Considering the different spatial scales of the model and data and the limited sampling time, the general trend is fairly well simulated using the diagnostic approach, especially over land. The strong correlation between N and sulfate indicated by the model in most regions suggests that the variability in N is underestimated. This is not surprising given the strong correlation between N and sulfate in the Tenerife observations that dominates the dataset used to derive (1a) and (1b). Since OM is probably underestimated in the dataset, N is more dependent on sulfate and a stronger correlation is exhibited between N and sulfate. On the other hand, correlations in the observations are expected to be lower than those in the model, given the
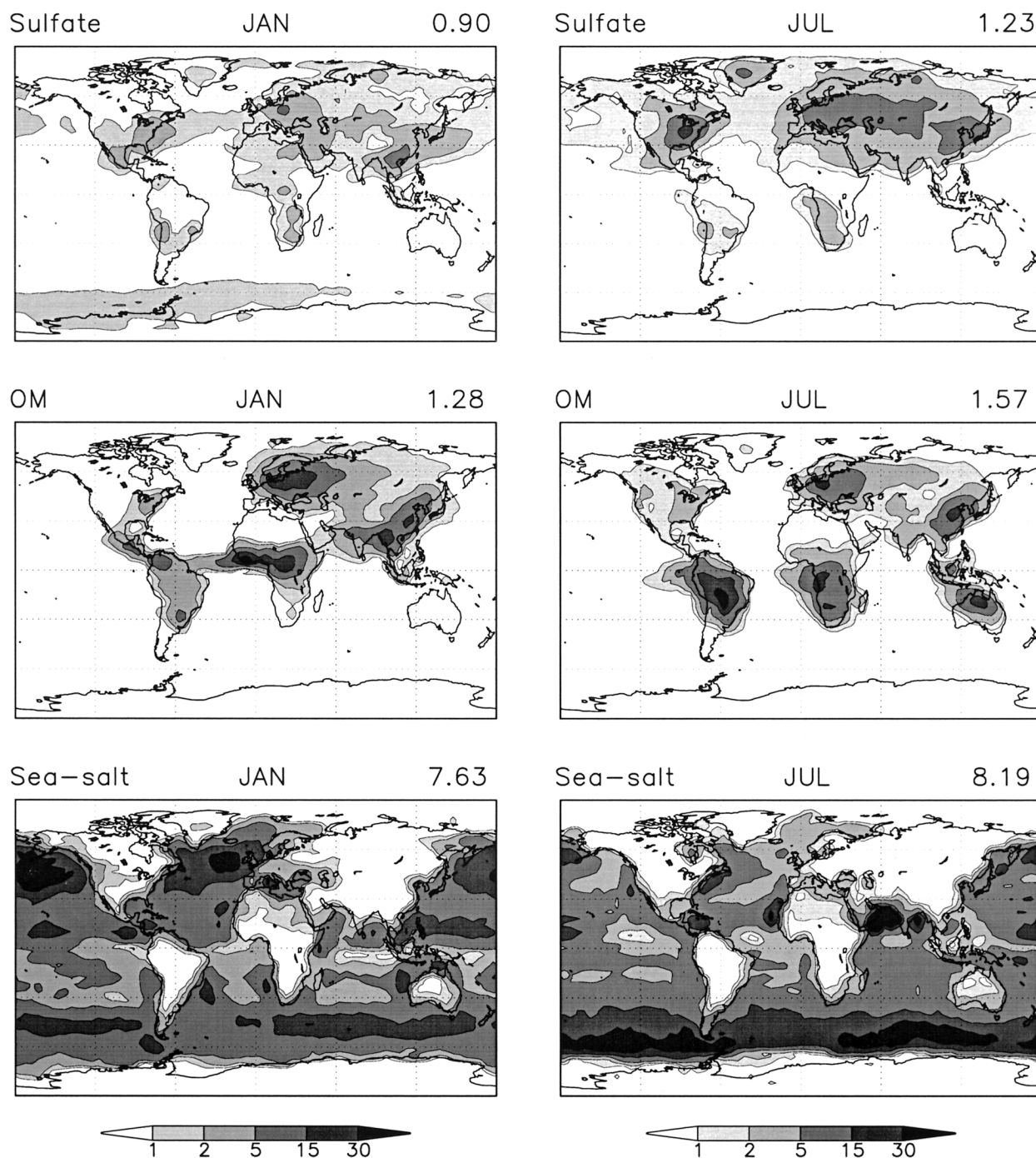
FIG. 1. Global distribution of sulfate, OM, and sea-salt mass (μg m^{-3}) in model layer 1 for Jan and Jul for the NEWCLD-M-5.0-P model run. Global annual averages are listed on the rhs.

significant observational errors and the small spatial scales sampled.

c. Aerosol indirect effect

Table 4 lists the global mean AIE values, and their partitioning by surface type and hemisphere for all five simulations. Included in the AIE is the relatively small ($\sim$0.1 W m^{-2}) longwave contribution. The spatial distributions of annual mean AIE are shown in Fig. 6. Changes in low cloud cover (ΔLCC) and liquid water path (ΔLWP) from PI to PD in the five experiments are also listed in Table 4.

Our global mean AIE values range from -1.55 to
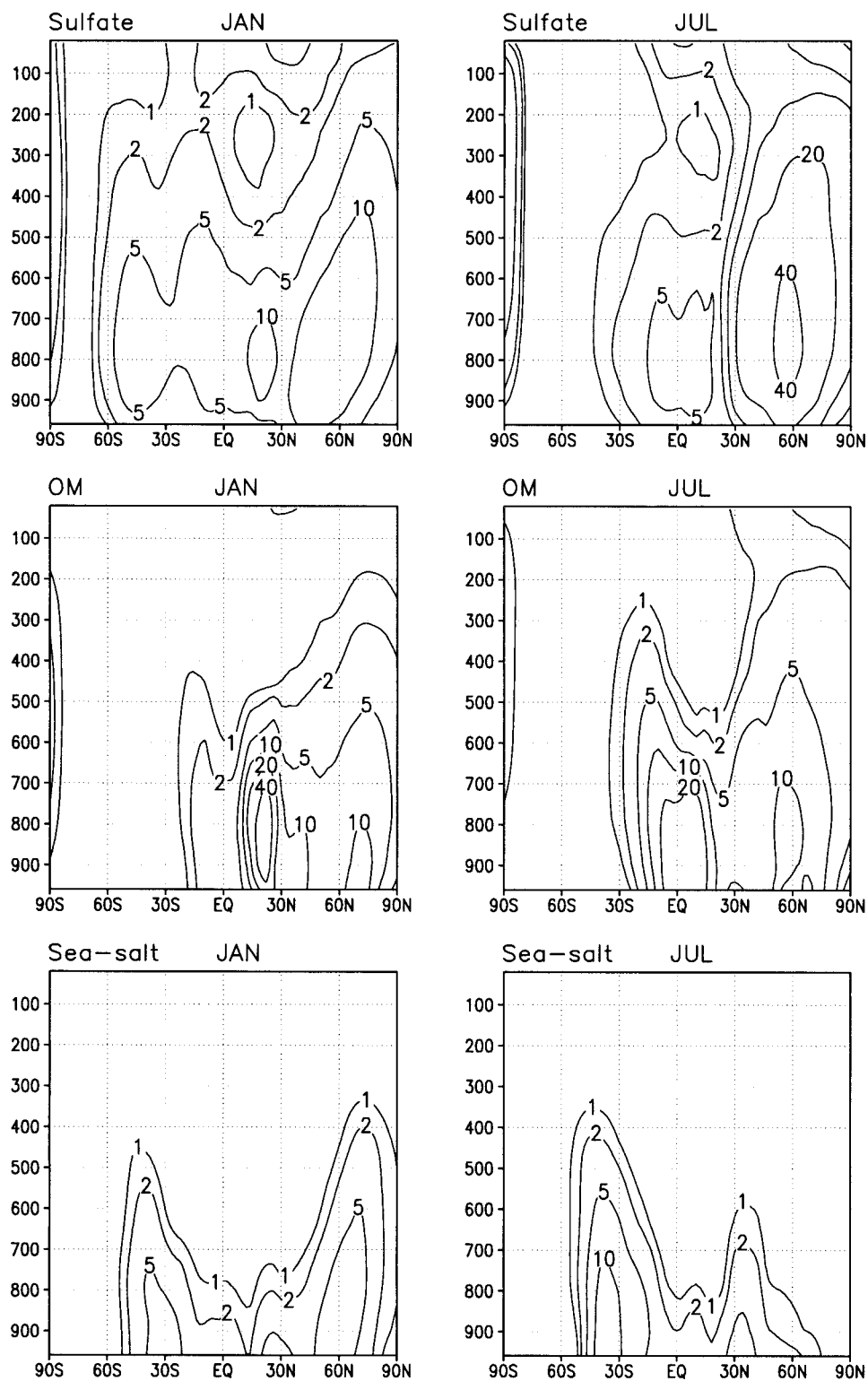
FIG. 2. Vertical distribution of sulfate (10^6 kg), OM (10^6 kg), and sea-salt (10^7 kg) mass for Jan and Jul for the NEWCLD-M-5.0-P model run.
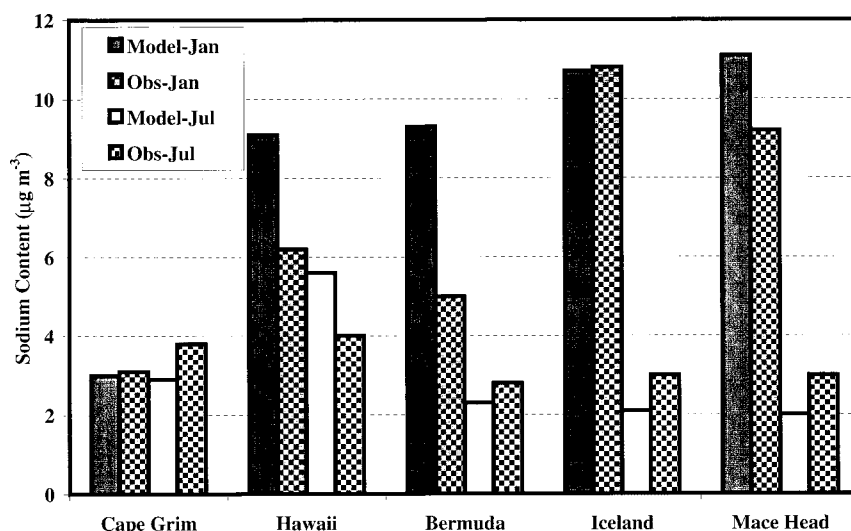
FIG. 3. Comparison between model simulated sodium content (obtained from the sea-salt concentrations) and observations at five locations for Jan and Jul for the NEWCLD-M-5.0-P model run.

-4.36 W m^{-2}, within the range of results reported for other GCMs but generally somewhat higher than typical values in previous studies. We also include in Table 4 an additional estimate for the AIE based on the difference in net radiation (NR) at top of atmosphere and the direct effect (DE; for both clear and cloudy skies), referred to as NR $-$ DE (Ghan et al. 2001a). The AIE is estimated from the difference in NR$-$DE between simulations with PD aerosols and that with PI aerosols. The two AIE estimates differ by less than $\sim$0.3 W m^{-2}. Neither estimate of the AIE is exact, because in a column in which both cloud and aerosol increase, the change in reflection of sunlight by the aerosol is partly due to the change in aerosol itself and partly due to the cloud-induced change in the availability of sunlight for the aerosol below (above) cloud to scatter. This can be counted as either part of the direct effect or the AIE and results in ambiguity in the AIE estimation. The cloud radiative forcing approach has the disadvantage that the sum of the direct and indirect effects does not exactly equal the change in net radiation, but it has the advantage of evaluating the cloud radiative impact in the realistic background in which it exists. The NR$-$DE approach gives an AIE and DE whose sum is exactly the change in net radiation, but it overestimates the AIE since the net radiation change due to clouds is estimated for an atmosphere without aerosols. Both methods are only approximate and the differences between them are small compared to the overall uncertainty in the AIE estimates.

A comparison of Tables 3 and 4 indicates that the AIE is more sensitive to the PI aerosol distribution than to the anthropogenic aerosol increase (with the one exception—NEWCLD-M-5.0). Since the PI burden in these runs varies only because of cloud physics as-

sumptions, it is also clear that the AIE is quite sensitive to uncertain aspects of cloud parameterization. In common with other models, the AIE is much stronger in the Northern Hemisphere than in the Southern Hemisphere, and the parameterization changes we test have little effect in the Southern Hemisphere in all but the most sensitive simulation. In all five simulations the AIE is stronger over land than over ocean, a feature we have in common with some previous investigators but not others. The differences between our results and previous workers are largely due to differences in the definition of the background aerosol and extent of aerosol–cloud interaction, as follows.

1) Our AIE is a true difference between simulated PD and PI conditions for all included aerosol types. Some previous studies prescribe an elevated continental background aerosol (to mimic other anthropogenic aerosols) and simulate only the AIE due to anthropogenic sulfate, which lowers the global AIE and shifts the maximum from land to ocean. Others use an N–sulfate regression with different slopes over land and ocean, which implicitly accomplishes the same thing. Others prescribe a lower limit for N, which can shift the peak AIE either onto land or ocean depending on where the lower limit is assumed to apply.

2) Some models use offline monthly mean sulfate fields to alter cloud properties but do not allow the clouds to feed back on the aerosol distribution. Our coupled model is fully interactive, and thus the global aerosol burden in the PI simulations can increase or decrease depending on cloud sources and sinks of aerosol. In general, the lower the PI aerosol burden, the larger the AIE.
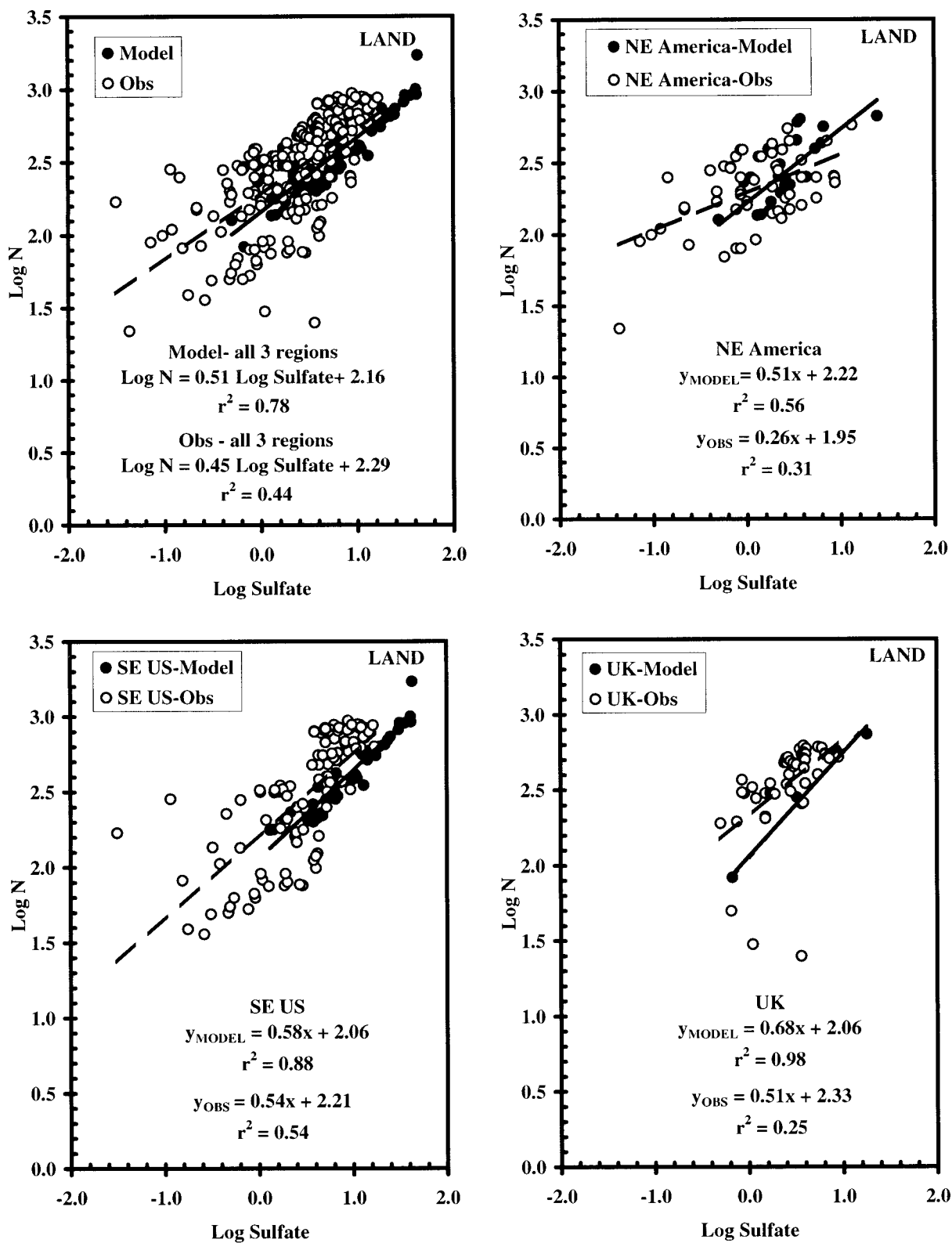
FIG. 4. Regression of N (cm^{-3}) predicted from the NEWCLD-M-5.0-P run vs the simulated sulfate mass (μg m^{-3}) for Jul for all land locations (topmost left panel) and for the three individual land locations. Also shown are the N–sulfate regressions from observations. The solid and dashed lines are the regression curves for model and observations, respectively.
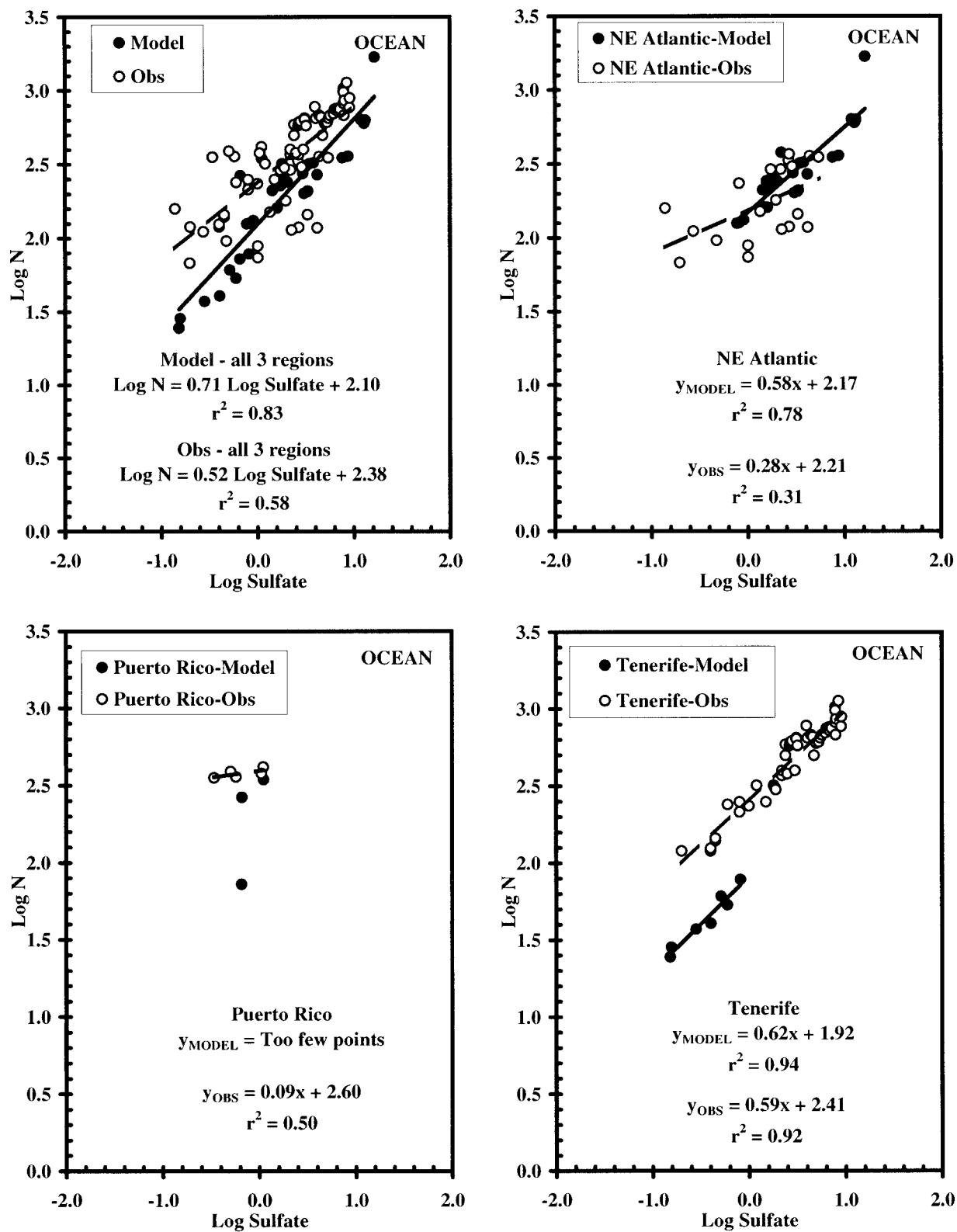
FIG. 5. Same as Fig. 4, but for ocean locations.

TABLE 4. Globally averaged annual means of the AIE evaluated by the model from the difference in cloud radiative forcing. Also included are the NH and SH, and land and ocean averages. NR−DE refers to the AIE calculated as the difference between net radiation and the direct aerosol effect. Global annual ΔLCC and ΔLWP between PD and PI emissions are also given.

Experiment	AIE (W m^{-2})					NR−DE (W m^{-2}) global	ΔLCC (%)	ΔLWP (g m^{-2})
	Land	Ocean	NH	SH	Global			
CTRL-R	−3.13	−1.31	−2.56	−1.09	−1.82	−1.95	0.15	−1.10
NEWCLD-R	−2.39	−1.22	−1.82	−1.27	−1.55	−1.72	0.22	−0.30
NEWCLD-M-7.5	−7.83	−2.99	−6.16	−2.56	−4.36	−4.68	1.18	7.80
NEWCLD-M-5.0	−2.91	−1.42	−2.39	−1.29	−1.84	−1.81	0.33	0.90
NEWCLD-M-5.0-P	−4.08	−1.75	−3.41	−1.41	−2.41	−2.53	0.56	1.90

3) Since the continental PI aerosol distribution cannot be observed, different assumptions about background sources can significantly influence the resulting AIE. For example, our control run assumes a 10% yield of OM from terpenes and produces an AIE of −1.82 W m^{-2}. A sensitivity test using a 5% yield instead reduces the background aerosol burden by 50% and increases the AIE to −2.56 W m^{-2}.

4) The GISS GCM surface winds are weaker than observed, and hence the model underestimate the sea–air transfer coefficient magnitude and the resulting DMS source when the Liss and Merlivat (1986) parameterization is employed. This may imply that our AIE over ocean is overestimated.

Comparing CTRL-R and NEWCLD-R illustrates the effect of the change in vertical cloud distribution. Shifting the low clouds upward by only 4 mb on average (but with a 10% absolute decrease in low-cloud contribution by the lowest layer) by itself reduces the magnitude of the AIE by 0.3 W m^{-2}. This occurs both because fewer of the clouds in NEWCLD-R are collocated with the altitude of largest anthropogenic aerosol increase, and because clouds in the lowest layer are most likely to rain, which explains the slightly lower aerosol burden in CTRL-R. Changes in LCC (0.15, 0.22%) and LWP (−1.1, −0.3 g m^{-2}) in these runs are due strictly to feedbacks, since they include only the first indirect effect, and are thus much smaller than those in the "M" runs, which allow for the second indirect effect.

Inclusion of the second indirect effect (NEWCLD-M-7.5) significantly increases the AIE relative to NEWCLD-R. However, the difference between these two cannot be interpreted as the magnitude of the second indirect effect itself, because qualitatively different autoconversion schemes were used in the two experiments. In general, the TC parameterization has much stronger autoconversion rates at typical cloud LWC values than the scheme used in Del Genio et al. (1996). As a result, the PI aerosol burden is very low in NEWCLD-M-7.5. This, combined with the actual second indirect effect, explains the exceptionally large overall AIE in this experiment. The runs with the TC scheme have annual mean global LWP values of 75–80 g m^{-2}, much closer to the satellite-retrieved value of 81 g m^{-2} reported by Greenwald et al. (1993) than the 118 g m^{-2} value in NEWCLD-R. The PI-to-PD increase in LWP (8 g m^{-2}) in NEWCLD-M-7.5 is about 10%, more than twice as large as the 4% relative (1.2% absolute) increase in LCC. Thus, the second indirect effect in our GCM is due to both cloud lifetime and in-cloud liquid water increases.

Since the TC scheme was designed for models that resolve clouds, the critical radius that initiates autoconversion is not a very physically meaningful parameter in the context of a global model, which is intended to represent an ensemble of clouds and a distribution of LWC values (Rotstayn 2000; Pincus and Klein 2000). NEWCLD-M-5.0 tests the sensitivity of the AIE to this effectively free parameter. By reducing the critical radius, we make autoconversion easier and thus limit the magnitude of the second indirect effect. The resulting decrease in magnitude of the AIE is dramatic (−4.36 to −1.84 W m^{-2}), not only because the anthropogenic changes in LCC (1.18% to 0.33%) and LWP (7.8 to 0.90 g m^{-2}) are smaller, but also because the efficient rainout

TABLE 5. Globally averaged Jul means for r_{eff}, N_c, $A-r_{eff}$ correlation, and column cloud susceptibility using the constant LWP assumption (CS$_1$) and column cloud susceptibility using the regression method (CS$_2$) that is, when LWP varies. Model results are compared to observations from Han et al. (1994, 1998a,b, 2000). also given are the AIE annual means.

Model/observations	AIE (W m^{-2})	r_{eff} (μm)	N_c (10^6 cm^{-2})	$A-r_{eff}$		CS$_1$ (10^{-8} cm^2)		CS$_2$ (10^{-8} cm^2)	
				$\tau \le 15$	$\tau > 15$	$\tau \le 15$	$\tau > 15$	$\tau \le 15$	$\tau > 15$
NEWCLD-R	−1.55	9.79	4.97	0.33	0.09	7.84	4.18	0.32	0.75
CTRL-R	−1.82	10.76	3.96	0.31	0.07	8.75	6.05	0.76	0.77
NEWCLD-M-5.0	−1.84	11.26	2.07	0.36	0.15	14.13	13.63	4.74	0.10
NEWCLD-M-5.0-P	−2.41	6.75	6.03	0.36	0.12	5.00	3.19	1.09	0.17
NEWCLD-M-7.5	−4.36	10.36	4.68	0.34	0.03	11.98	6.35	3.01	0.40
Observations	—	11.44	4.43	0.30	−0.19	8.29	2.70	3.19	1.15
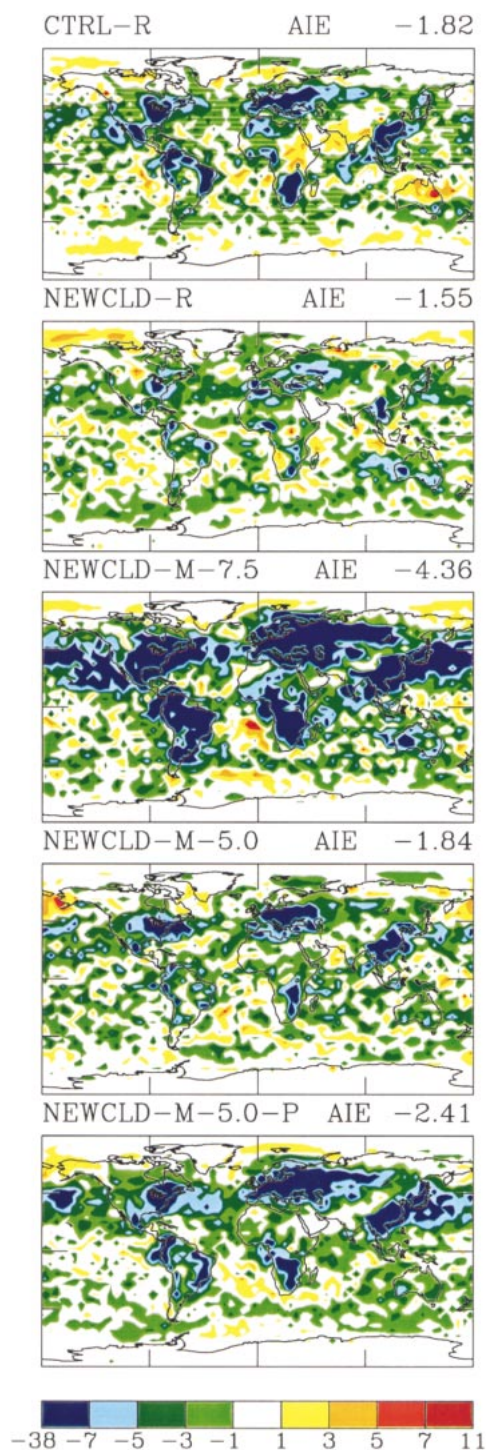
causes the anthropogenic increase in aerosol burden to be much less in this experiment than in the other four.

The aerosol burden in NEWCLD-M-7.5 and especially NEWCLD-M-5.0 is significantly lower than that in the earlier version of the coupled model analyzed in detail by Koch et al. (1999), which did not include the AIE. Although the actual global aerosol burden is unknown, the earlier model did compare reasonably well with point observations at a variety of locations. At the same time, the scavenging scheme in that model assigns too large a precipitating area of clouds compared to satellite observations. NEWCLD-M-5.0-P thus weakens the scavenging to offset the effect of the stronger autoconversion in the TC scheme. The resulting PI aerosol burden is much larger, and the PD burden is much closer to that in Koch et al. (1999). Thus, even though the PD aerosol burden is the largest of all five experiments and both indirect effects are included, the total AIE is only -2.41 W m^{-2}. Changes in LCC (0.6%) and LWP (2 g m^{-2}) are intermediate between the other M experiments.

5. Comparisons with satellite data

Han et al. (1994, 1998a,b, 2000) have retrieved a variety of parameters that are potentially diagnostic of aerosol–cloud interactions from global satellite datasets. In this section we compare analogous model parameters to these retrievals to determine whether the satellite diagnostics constrain the AIE. Model outputs were processed in the same way as were the satellite retrievals, with only clouds with tops warmer than 273 K included and parameters calculated either at cloud top or as column integrals as appropriate. Table 5 summarizes the global mean results for July, in increasing order of the simulated AIE magnitude, while Figs. 7–9 show the global distributions of each parameter for the observations and for three simulations that span the range of AIE values in the GCM. Impressions gained from January comparisons (not shown) were generally similar.

a. Droplet effective radius and column number concentration

Figure 7 shows the distributions of r_{eff} (left) and column droplet number concentration N_c. Particle size is proportional to $(LWC/N)^{1/3}$ and column number concentration is the vertical integral of N, so we might expect changes in r_{eff} and N_c from one experiment to another to be negatively correlated. Table 5 shows that with the exception of the extreme high AIE experiment NEWCLD-M-7.5, this is the case. In the other four simulations, N_c is primarily controlled by the aerosol burden (compare with Table 3). In general r_{eff} is underpredicted by the model. In part, this may be explained by the fact that the satellite-retrieved radius is characteristic of only the top $\tau \approx 1$ of the cloud. Since LWC increases with height in nonprecipitating clouds, the cloud-top droplet sizes tend to be larger than the mean throughout the cloud. The GCM's cloud-top value is the mean for the highest cloud layer, which in many cases is the entire depth of the cloud.

The GCM does produce the sense of particle size differences over land and ocean. Its NH–SH differences are
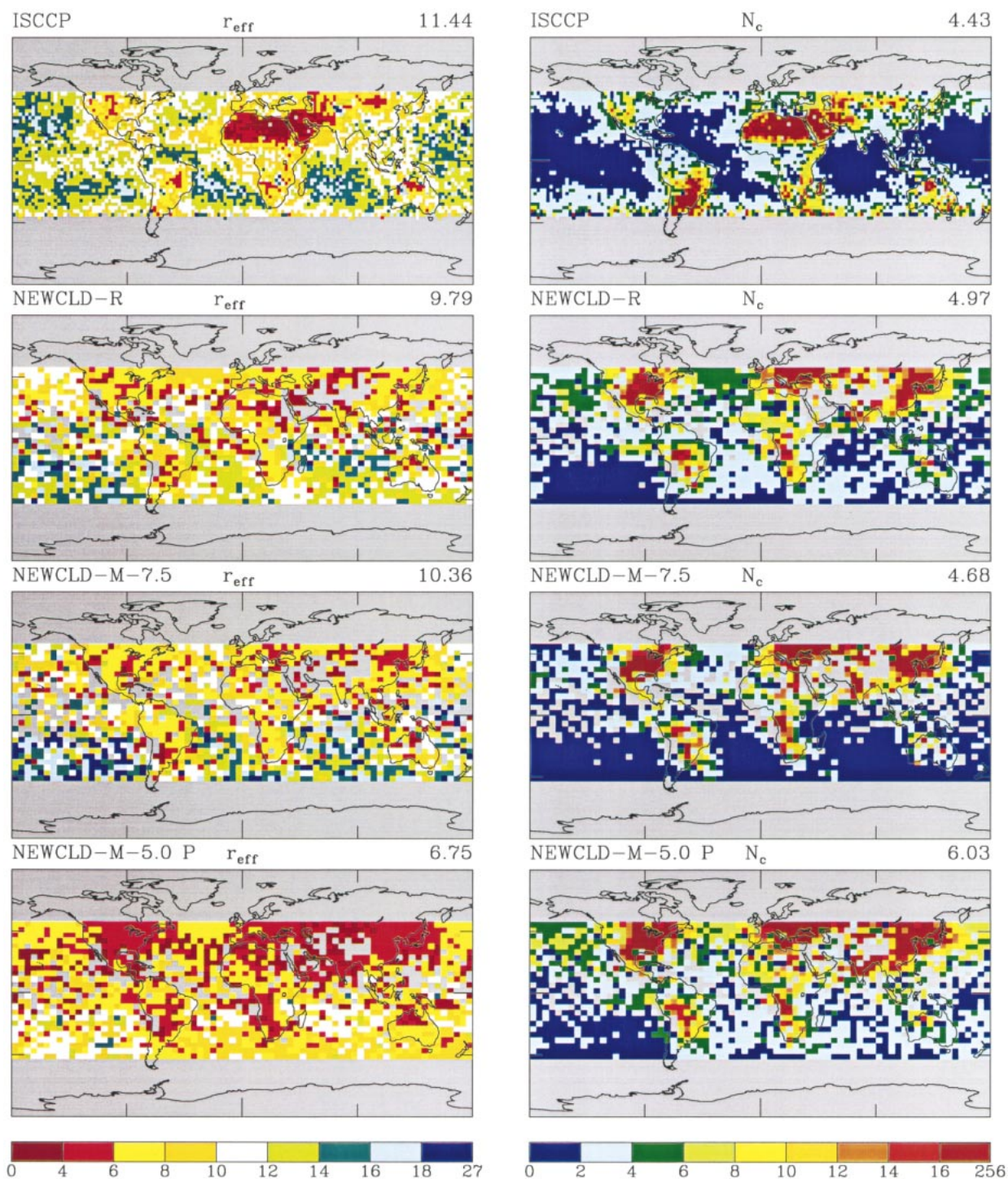
FIG. 7. Global distribution of model-simulated r_{eff} (μm) and N_c (10^6 cm^{-2}) for three of the five model runs listed in Table 2. ISCCP observations from Han et al. (1994, 1998b) are also shown (topmost panels). Global averages are listed on the rhs.

much greater than the satellite-retrieved values, in part because the model aerosol impact appears to be too large over NH midlatitude oceans, and in part because the satellite retrievals include some regions of unusually small particle sizes over SH desert regions that are probably dust

contamination. Here, N_c is somewhat overestimated over NH land and slightly underestimated over SH land in most of the simulations. Several of the runs produce ocean concentrations similar to those observed, but the observed ocean minima tend to be at low latitudes, while the model

ocean minima are in southern midlatitudes. The AIE does not vary consistently with either r_{eff} or N_c, so although they represent one component of a model validation strategy, neither parameter by itself can be considered a diagnostic of the AIE.

b. Albedo–particle size correlations

Since the AIE is largely a response of cloud albedo to aerosol-induced changes in cloud droplet number and size, it is potentially more fruitful to relate albedo variations to changes in either quantity than to utilize the mean quantities themselves. Han et al. (1998a) correlated albedo to droplet effective radius in the hope of finding regional signatures of the AIE. They found the expected negative relationship (brighter clouds with smaller particle sizes) only for the optically thickest ($\tau > 15$) 15%–20% of all low clouds. For the majority of low clouds, albedo is positively correlated with particle size. This occurs because for thinner clouds, dynamically induced changes in LWC control particle size, hiding any AIE in such clouds amidst the much larger natural variability. For the thicker clouds, on the other hand, the onset of precipitation may limit LWC increases and allow the weak AIE signal to emerge (Nakajima and Nakajima 1995; Lohmann et al. 2000).

Cloud albedo (A) in the GCM was estimated from the calculated optical thickness using $A = (1 - g)\tau/[2 + (1 - g)\tau]$, where $g = 0.85$ is the asymmetry parameter for single scattering. The GCM produces albedo–particle size correlations for the thinner clouds that are quite close to those observed (Table 5; Fig. 8, left). There is little variation from one simulation to another, supporting the idea that the correlation for these clouds is mostly due to natural variability and not aerosol. The GCM also simulates much smaller correlations overall and some regions of negative albedo–particle size correlation for the thicker clouds, although in no case is the GCM global mean correlation for the thicker clouds negative as is true for the satellite data. Even though the lowest albedo–r_{eff} correlations occur in the run with the highest AIE and the negative correlations in all runs are a lot more pronounced in clouds in model layer 1 where the aerosol effect is the strongest, an inverse relation between albedo–r_{eff} and the AIE is not observed in Table 5. Thus, although this satellite relation may offer some evidence of the AIE, it is apparently not sensitive enough to distinguish between large and small AIE simulations in our model.

c. Column susceptibility

Twomey (1991) first suggested that the albedos of cleaner clouds with smaller N are more susceptible to changes in N than are clouds with larger N. If LWC, cloud physical thickness, and the droplet size distribution are held constant, then the susceptibility $dA/dN = A(1 - A)/(3N)$. This relationship has been used to

evaluate the sensitivity of clouds to aerosols in different regions (Taylor and McHaffie 1994; Platnick and Twomey 1994). Cloud droplet numbers concentration is not observed by satellites, but Han et al. (2000) have retrieved an analogous column cloud susceptibility defined for constant LWP as $CS_1 = dA/dN_c = A(1 - A)/(3N_c)$. Furthermore, since LWP and size distribution need not remain constant, Han et al. provide another estimate of column susceptibility $CS_2 = \Delta A/\Delta N_c$ by regressing A versus N_c.

Figure 9 shows both versions of column susceptibility for thinner clouds, while Table 5 indicates the global mean values for thinner and thicker clouds separately. Excepting once again the extreme case NEWCLD-M-7.5, differences in global mean CS_1 values are inversely correlated with differences in N_c, and thus CS_1 provides no independent information about cloud–aerosol interactions. Likewise, model-data differences in the global distribution of CS_1 mimic the differences already described for N_c.

To estimate CS_2 in the GCM, A, and N_c values were sampled every 6 h to capture synoptic variability, and gridboxes with fewer than 10 points of warm cloud occurrences over the month were excluded from the regression analysis. Like Han et al., we find that susceptibilities are noticeably lower when LWP is not assumed fixed, although our susceptibilities are significantly smaller than those retrieved by Han et al. in three of the five simulations. The GCM especially underestimates susceptibility over the oceans, and although the model produces some gridpoints with negative susceptibilities, they are randomly scattered over the oceans rather than being confined to the eastern ocean marine stratus regions as in the satellite data. Susceptibilities are higher for the runs that include the second indirect effect than for the runs that simulate only the first indirect effect. Also, the decrease in CS_2 from thin to thick clouds (as in observations) are only seen for the M runs, suggesting that microphysics plays a bigger role in determining cloud susceptibility than does radiation. Furthermore, for the three runs that include the second indirect effect, both susceptibilities increase (for the optically thin cases) as the aerosol burden decreases, as we might expect, but this is not a predictor of the resulting AIE because of differences in PI aerosol.

6. Discussion and conclusions

Our suite of simulations differs from those performed by previous workers in that we emphasize sensitivity of the AIE to uncertain cloud parameterization elements (formation, autoconversion, scavenging) that affect major source and sink terms in the aerosol budgets. We did not perform any tuning, so our global aerosol burdens vary considerably among the different simulations (Table 3). The global burdens of all aerosol types are poorly constrained, since only point observations in some parts of the world are available, with little vertical
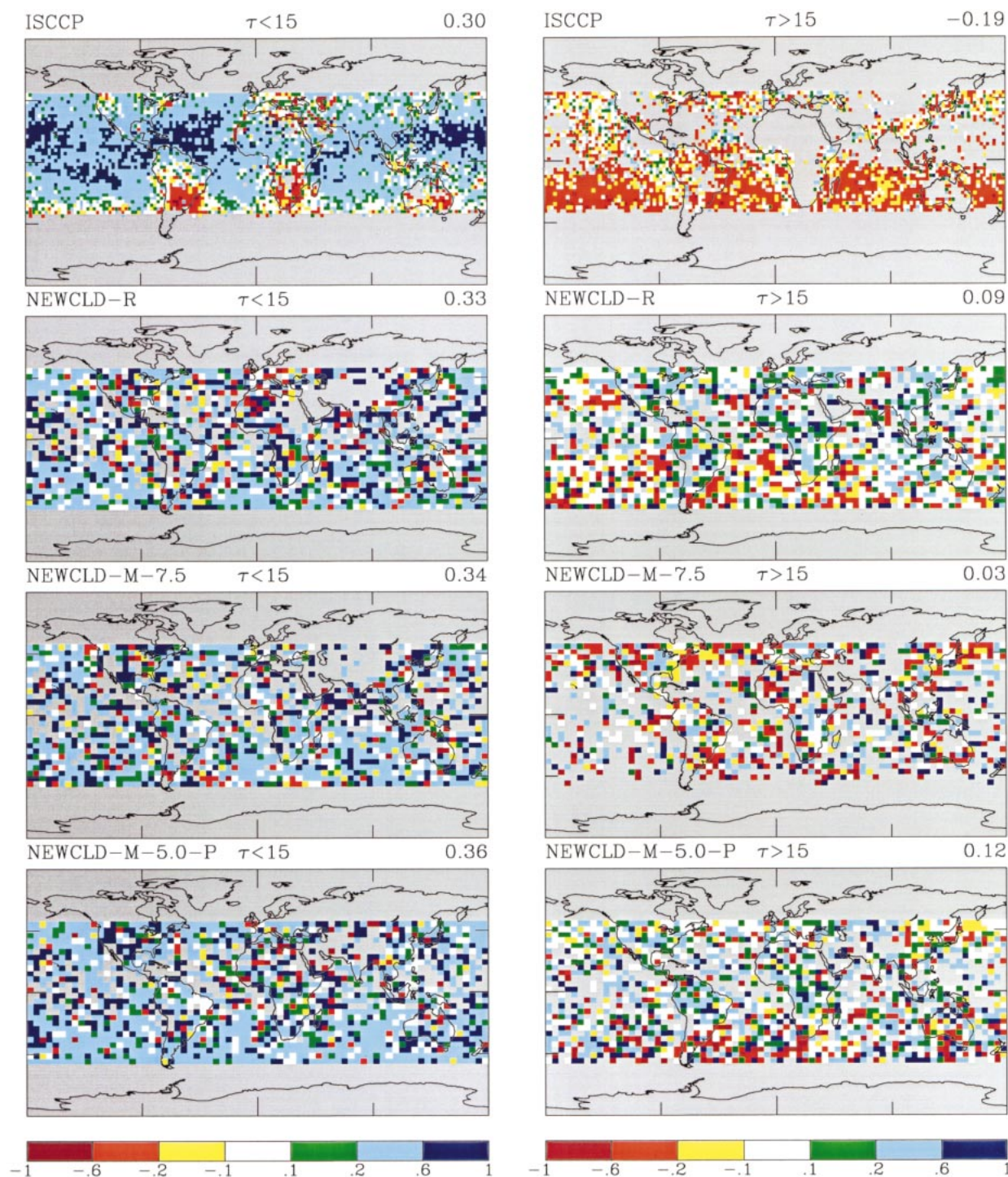
FIG. 8. Global distribution of the correlation coefficient between cloud albedo and r_{eff} for optically thin ($\tau \le 15$) and thick ($\tau > 15$) clouds for Jul for three of the five model runs listed in Table 2. ISCCP observations from Han et al. (1998a) are also shown (topmost panels). Global averages are listed on the rhs.

profile information. The sulfur burdens in existing models range over about a factor of two (Koch et al. 1999). Two of our simulations (NEWCLD-M-7.5, NEWCLD-M-5.0) have very low aerosol burdens that are probably inconsistent with available data, but the other three are representative of the range found in other models.

Of even more importance is that the PI aerosol distribution is and will remain completely unconstrained
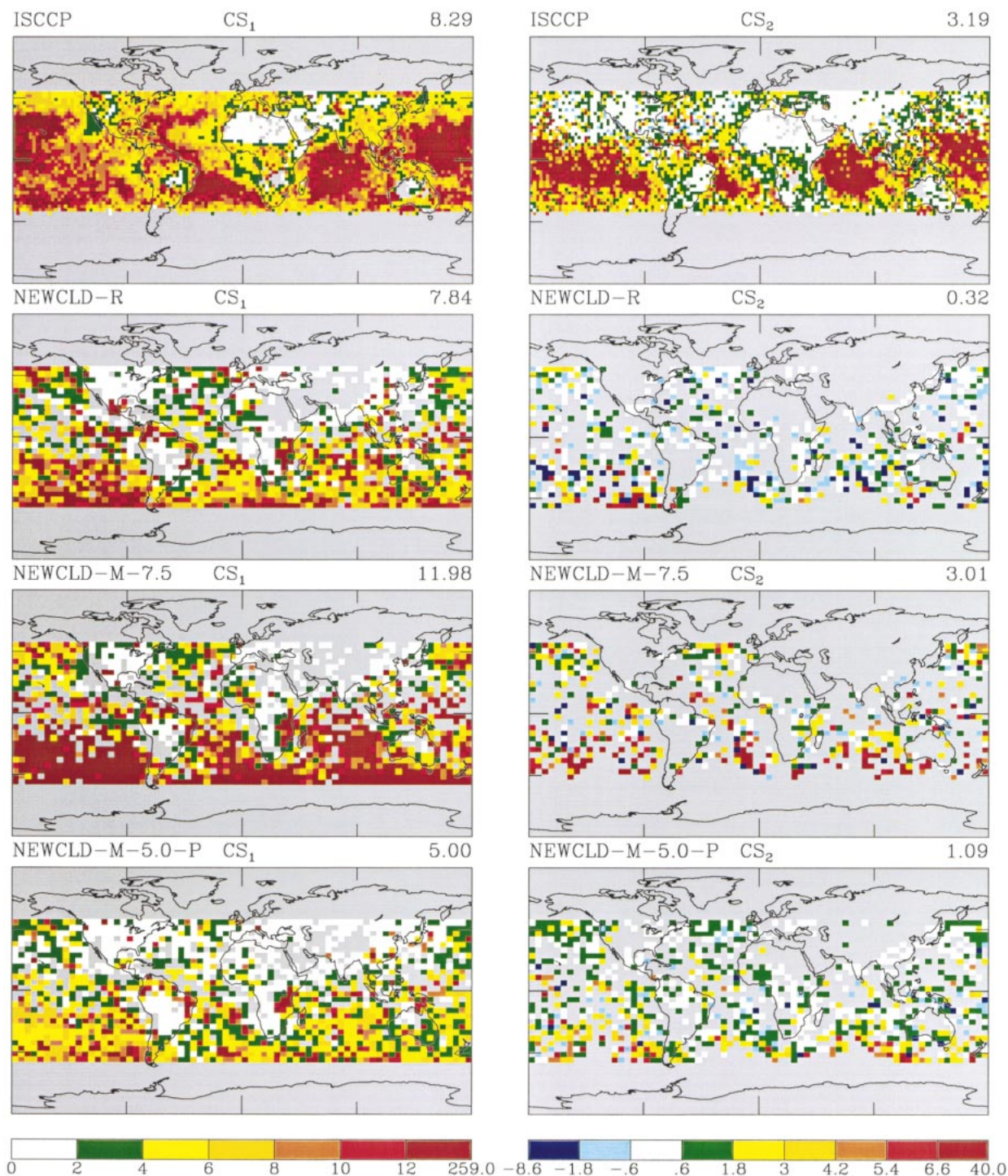
FIG. 9. Global distribution of the column cloud susceptibility (10^{-8} cm^2) calculated using the constant LWP assumption, referred to as CS$_1$, and under varying LWP assumption, referred to as CS$_2$, for optically thin ($\tau \leq 15$) clouds in Jul for three of the five model runs listed in Table 2. ISCCP observations from Han et al. (2000) are also shown (topmost panels). Global averages are listed on the rhs.

by observations. The combined uncertainty in PD and PI aerosol burden is the single largest uncertainty factor for the AIE in our model. As a crude indicator of their impact, we plot in Fig. 10 the AIE versus the ratio of

PD to PI sulfate burden. (A similar plot using PD and PI sulfate + OM gives similar results, since sulfate is more abundant and dominates the regression we use.) In our limited sample of model runs, the magnitude of
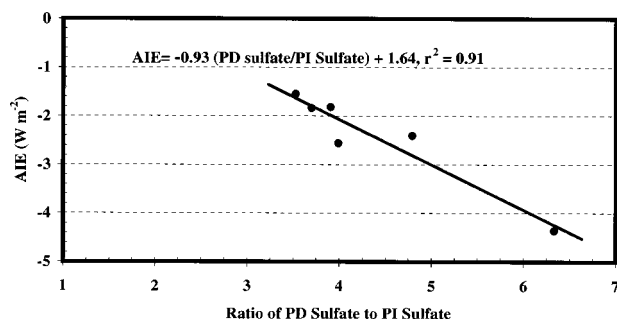
FIG. 10. Model simulations of the AIE (W m^{-2}) vs the ratio of PD to PI sulfate aerosol burden for the five model runs listed in Table 2 and an additional sensitivity run (same as the CTRL-R run but with a 50% reduction in the PI organic aerosol burden).

the AIE is strongly correlated with the fractional enhancement of aerosol burden by anthropogenic activities. Thus, we can weaken/strengthen the AIE by increasing/decreasing the PI burden, and to a lesser extent by decreasing/increasing the PD burden.

The sensitivity to the PI burden may partly explain the absence of any weak AIE results in our set of simulations. Specifically, the GISS GCM's DMS source is significantly weaker than that of other models because of the GCM's weak surface winds; Koch et al. (1999) report a 42% increase in the DMS source when the model is forced by special sensor microwave/imager winds instead. Applying such a change to Fig. 10, we anticipate that our AIE might decrease in magnitude by a few tenths of a watts per meters squared if this were corrected. Other sources such as the OM yield from terpenes increase the uncertainty. Even more importantly, the microphysical processes that remove aerosols in GCMs can drastically alter the aerosol burden, and proper representations of these processes that account for subgrid LWC variability do not exist (Pincus and Klein 2000). It is clear that using offline noninteractive aerosol fields to force a GCM misses important feedbacks of the clouds on the aerosol field.

Since it is impossible to specify the PI aerosol burden accurately and uniformly across models, GCM estimates of the AIE can be expected not to converge as long as PI conditions are used as the baseline. Since the total AIE from the start of the Industrial Revolution is of less practical importance than the recent and future rate of increase of the AIE, we suggest a shift in model strategy that focuses on simulating the change in AIE over the period for which the most reliable observations exist. If the National Aeromatics and Space Administration (NASA) Global Aerosol Climatology Project can generate an aerosol climatology for the past two decades with reasonable accuracy, this time period might serve as a better standard for different GCMs to operate on common ground, so that remaining disagreements might more easily be traced to differences in model physics. Such a strategy might enhance the usefulness of satellite products as well. None of the tested satellite diagnostics

constrains the AIE in our simulations (Table 5). However, much of the simulated variability in AIE in our model results from PI aerosol burden variations, which are unrelated to the current climate aerosol–cloud sensitivity captured in the data.

Of more concern for observationally constraining the AIE is the fact that aerosols appear to have a subtle effect on clouds that is largely obscured by natural meteorological variability. Thus, unlike the global mean greenhouse gas or direct aerosol forcing, neither of which is greatly affected by dynamics, it will never be possible to simply estimate the global AIE by using "observed" aerosol modifications of clouds as input to a one-dimensional radiative transfer calculation. What is needed is to combine the existing satellite products with meteorological analysis fields to isolate specific dynamical regimes within which the cloud variability due to aerosols might be detected. A similar analysis applied to a GCM might then be able to validate the GCM's process representations, and such a model might then give a credible estimate of the AIE. In other words, the AIE, which is usually grouped with climate forcings, is more properly treated as a feedback that can only be estimated within the model context.

Our study also highlights some needed observations. Since aerosol concentrations decrease sharply with height, it is important to accurately simulate the detailed vertical distributions of clouds. Coarse vertical resolution models such as the one we use must clearly be replaced with versions that adequately portray inversions, decoupled boundary layers, and cloud turbulence strength. Observations to validate such models are lacking, though. ISCCP gives a first-order global estimate of low cloud height but apparently contains biases in marine stratus regions (Wang et al. 1999). Collocated vertical profiles of cloud and aerosol at a number of locations from surface lidars and radars may offer the best hope of getting such information. Future field experiments can be justified, but only if they sample climate regimes unobserved thus far, especially in regions where other aerosols dominate sulfate, and only if they measure N and all relevant aerosols and include supporting large-scale and turbulence-scale meteorological information.

Finally, it is instructive to compare the status of AIE simulations to that of cloud feedback. The range of cloud feedback estimates broadened considerably 10–15 yr ago as new physics was introduced that increased the number of possible feedback loops. Only recently have observations begun to narrow that range. Diagnostic cloud schemes ultimately gave way to prognostic cloud water parameterizations, not just because they represent better physics but because they allow GCMs to predict not only sources but also important sinks of cloud water, which require the memory of the previous cloud state. AIE simulations, by comparison, have existed for fewer than 10 yr. The range of estimates has recently expanded, and no observational constraints

have yet been identified that narrow the range. Prognostic schemes have begun to appear, but their ultimate fate will depend on whether droplet concentrations and particle sizes on GCM-resolved space scales and timescales can be shown to deviate in important ways from equilibrium with the simulated aerosol field. For the foreseeable future, diagnostic approaches offer comparable predictive capability for estimates of the AIE.

REFERENCES

Albrecht, B. A., 1989: Aerosols, cloud microphysics, and fractional cloudiness. *Science,* **245,** 1227–1230.

Andreae, M. O., and P. J. Crutzen, 1997: Biogeochemical sources and role in atmospheric chemistry. *Science,* **276,** 1052–1058.

Baughcum, S. L., D. M. Chan, S. M. Happenny, S. C. Henderson, P. S. Hertel, T. Higman, D. R. Maggiora, and C. A. Oncina, 1993: Emissions scenario development: Schedules 1990 and projected subsonic, Mach 2.0 and Mach 2.4 aircraft. Atmospheric Effects of Stratospheric Aircraft: A Third Report, NASA Publ. 1313, 89–131.

Benkovitz, C. M., and Coauthors, 1996: Global gridded inventories of anthropogenic emissions of sulfur and nitrogen. *J. Geophys. Res.,* **101,** 29 239–29 253.

Borys, R. D., D. H. Lowenthal, M. A. Wetzel, F. Herrera, A. Gonzalez, and J. Harris, 1998: Chemical and microphysical properties of marine stratiform cloud in the North Atlantic. *J. Geophys. Res.,* **103,** 22 073–22 085.

Boucher, O., 1995: GCM estimate of the indirect aerosol forcing using satellite-retrieved droplet effective radii. *J. Climate,* **8,** 1403–1409.

——, and U. Lohmann, 1995: The sulphate-CCN-cloud albedo effect. A sensitivity study using two general circulation models. *Tellus,* **47B,** 281–300.

——, H. LeTreut, and M. B. Baker, 1995: Precipitation and radiation modeling in a general circulation model: Introduction of cloud microphysical processes. *J. Geophys. Res.,* **100,** 16 395–16 414.

Brenguier, J. L., H. Pawlowska, L. Schueller, R. Preusker, J. Fischer, and Y. Fouquart, 2000: Radiative properties of boundary layer clouds: Droplet effective radius versus number concentration. *J. Atmos. Sci.,* **57,** 803–821.

Charlson, R. J., J. D. S. Covert, and T. V. Larson, 1984: Observation of the effect of humidity on light scattering by aerosols. *Hygroscopic Aerosols,* L. Ruhnke and A. Deepak, Eds., A. Deepak Publishing, 35–44.

——, J. E. Lovelock, M. O. Andreae, and S. G. Waren, 1987: Oceanic phytoplankton, atmospheric sulphur, cloud albedo and climate. *Nature,* **326,** 655–661.

Cheng, Y., V. M. Canuto, and A. M. Howard, 2002: An improved model for the turbulent PBL. *J. Atmos. Sci.,* in press.

Chuang, C. C., J. E. Penner, K. E. Taylor, A. S. Grossmann, and J. J. Walton, 1997: An assessment of the radiative effects of anthropogenic sulfate. *J. Geophys. Res.,* **102,** 3761–3778.

Coakley, J. A., Jr., R. L. Bernstein, and P. A. Durkee, 1987: Effect of ship-track effluents on cloud reflectivity. *Science,* **237,** 1020–1022.

——, and Coauthors, 2000: The appearance and disappearance of ship tracks on large spatial scales. *J. Atmos. Sci.,* **57,** 2765–2778.

Cooke, W. F., C. Liousse, H. Cachier, and J. Feichter, 1999: Construction of a 1° × 1° fossil fuel emission data set for carbonaceous aerosol and implementation and radiative impact in the ECHAM4 model. *J. Geophys. Res.,* **104,** 22 137–22 162.

Del Genio, A. D., and M.-S. Yao, 1993: Efficient cumulus parameterization for long-term climate studies: The GISS scheme. *Representation of Cumulus Convection in Numerical Models, Meteor. Monogr.,* No. 46, Amer. Meteor. Soc., 181–184.

——, ——, and K. K.-W. Lo, 1996: A prognostic cloud water parameterization for global climate models. *J. Climate,* **9,** 270–304.

Durkee, P. A., and Coauthors, 2000: The impact of ship-produced aerosols on the microstructure and albedo of warm marine stratocumulus clouds: A test of MAST hypotheses 1i and 1ii. *J. Atmos. Sci.,* **57,** 2554–2569.

Ferek, R. J., and Coauthors, 2000: Drizzle suppression in ship tracks. *J. Atmos. Sci.,* **57,** 2707–2728.

Ghan, S. J., G. Guzman, and H. Abdul-Razzak, 1998: Competition between sea salt and sulfate particles as cloud condensation nuclei. *J. Atmos. Sci.,* **55,** 3340–3347.

——, and Coauthors, 2001a: A physically-based estimate of radiative forcing by anthropogenic sulfate aerosol. *J. Geophys. Res.,* **106,** 5279–5293

——, ——, J. Hudson, and F.-M. Breon, 2001b: Evaluation of aerosol indirect forcing in MIRAGE. *J. Geophys. Res.,* **106,** 5317–5334

Gong, S. L., L. A. Barrie, and J.-P. Blanchet, 1997a: Modeling sea-salt aerosols in the atmosphere. Part 1: Model development. *J. Geophys. Res.,* **102,** 3805–3818.

——, J. M. Prospero, D. L. Savoie, G. P. Ayers, J.-P. Blanchet, and L. Spacek, 1997b: Modeling sea-salt aerosols in the atmosphere. Part 1: Atmospheric concentrations and fluxes. *J. Geophys. Res.,* **102,** 3819–3830.

Greenwald, T. J., G. L. Stephens, T. H. Vonder Haar, and D. L. Jackson, 1993: A physical retrieval of cloud liquid water over the global oceans using special sensor microwave/imager (SSM/I) observations. *J. Geophys. Res.,* **98,** 18 471–18 488.

Guenther, A., and Coauthors, 1995: A global model of natural volatile organic compound emissions. *J. Geophys. Res.,* **100,** 8873–8892.

Han, Q., W. B. Rossow, and A. A. Lacis, 1994: Near-global survey of effective droplet radii using ISCCP data. *J. Climate,* **7,** 465–497.

——, ——, J. Chou, and R. M. Welch, 1998a: Global survey of the relationships of cloud albedo and liquid water path with cloud droplet size using ISCCP. *J. Climate,* **11,** 1516–1528.

——, ——, ——, and ——, 1998b: Global variations of column droplet concentration in low-level clouds. *Geophys. Res. Lett.,* **25,** 1419–1422.

——, ——, ——, and ——, 2000: Near-global survey of cloud column susceptibility using ISCCP data. *Geophys. Res. Lett.,* **27,** 3221–3224.

Hansen, J. E., and L. D. Travis, 1974: Light scattering in planetary atmospheres. *Space. Sci. Rev.,* **16,** 527–610.

——, G. Russell, D. Rind, P. Stone, A. Lacis, S. Lebedeff, R. Ruedy, and L. Travis, 1983: Efficient three-dimensional global models for climate studies: Models I and II. *Mon. Wea. Rev.,* **111,** 609–662.

——, M. Sato, and R. Ruedy, 1997: Radiative forcing and climate response. *J. Geophys Res.,* **102,** 6831–6864.

——, ——, ——, A. Lacis, and V. Oinas, 2000: Global warming in the twenty-first century: An alternative scenario. *Proc. Natl. Acad. Sci. USA,* **97,** 9875–9880.

Jones, A., D. L. Roberts, and A. Slingo, 1994: A climate model study of indirect radiative forcing by anthropogenic sulphate aerosols. *Nature,* **370,** 450–453.

Kaufman, Y. J., and R. S. Fraser, 1997: The effect of smoke particles on clouds and climate forcing. *Science,* **277,** 1636–1639.

Kettle, A. J., and M. O. Andreae, 2000: Flux of DMS from the oceans: A comparison of updated data sets and flux models. *J. Geophys. Res.,* **105,** 26 793–26 808.

——, and Coauthors, 1999: A global database of sea surface dimethyl-sulfide (DMS) measurements and a procedure to predict sea surface DMS as a function of latitude, longitude and month. *Global Biogeochem. Cycles,* **13,** 394–444.

Kiehl, J. T., T. L. Schneider, P. J. Rasch, M. C. Barth, and J. Wong, 2000: Radiative forcing due to sulfate aerosols from simulations with the NCAR Community Climate Model. *J. Geophys. Res.,* **105,** 1441–1457.

King, M. D., L. F. Radke, and P. V. Hobbs, 1993: Optical properties of marine stratocumulus clouds modified by ships. *J. Geophys. Res.,* **98,** 2729–2739.

Koch, D., 2001: The transport and direct radiative forcing of carbonaceous and sulfate aerosols in the GISS GCM. *J. Geophys. Res.* **106,** 20 311–20 332

——, D. Jacob, I. Tegen, D. Rind, and M. Chin, 1999: Tropospheric sulfur simulation and sulfate direct radiative forcing in the GISS GCM. *J. Geophys. Res.,* **104,** 23 799–23 822.

Kogan, Z. N., Y. L. Kogan, and D. K. Lilly, 1997: Cloud factor and seasonality of the indirect effect of anthropogenic sulfate aerosols. *J. Geophys. Res.,* **102,** 25 927–25 939.

Leaitch, W. R., G. A. Isaac, J. W. Strapp, C. M. Banic, and H. A. Wiebe, 1992: The relationship between cloud droplet number concentration and anthropogenic pollution: Observations and climatic implications. *J. Geophys. Res.,* **97,** 2463–2474.

——, and Coauthors, 1996: Physical and chemical observations in marine stratus during the 1993 North Atlantic Regional Experiment: Factors controlling cloud droplet number concentration. *J. Geophys. Res.,* **101,** 29 123–29 135.

Lin, B., and W. B. Rossow, 1997: Precipitation water path and rainfall rate estimates over oceans using special sensor microwave imager and International Satellite Cloud Climatology Project data. *J. Geophys. Res.,* **102,** 9359–9374.

Liousse, C., J. E. Penner, C. Chuang, J. J. Walton, H. Eddleman, and H. Cachier, 1996: A global three-dimensional model study of carbonaceous aerosols. *J. Geophys. Res.,* **101,** 19 411–19 432.

Liss, P. S., and L. Merlivat, 1986: Air–sea exchange rates: Introduction and synthesis. *The Role of Air–Sea Exchange in Geochemical Cycling,* P. Buat-Menard, Ed., D. Reidel, 113–127.

Liu, P. S. K., W. R. Leaitch, C. M. Banic, S.-M. Li, D. Ngo, and W. J. Megaw, 1996: Aerosol observations at Chebogue Point during the 1993 North Atlantic Regional Experiment: Relationships among cloud condensation nuclei, size distribution and chemistry. *J. Geophys. Res.,* **101,** 28 971–28 990.

Lohmann, U., and J. Feichter, 1997: Impact of sulphate aerosols on albedo and lifetime of clouds: A sensitivity study with the ECHAM4 GCM. *J. Geophys. Res.,* **102,** 13 685–13 700.

——, ——, C. C. Chuang, and J. E. Penner, 1999: Predicting the number of cloud droplets in the ECHAM GCM. *J. Geophys. Res.,* **104,** 9169–9198.

——, G. Tselioudis, and C. Tyler, 2000: Why is the cloud-albedo particle size relationship different in optically thick and optically thin clouds? *Geophys. Res. Lett.,* **27,** 1099–1102.

Mace, G. G., C. Jakob, and K. P. Moran, 1998: Validation of hydrometeor occurrence predicted by the ECMWF model using millimeter wave radar data. *Geophys. Res. Lett.,* **25,** 1645–1648.

Matsumoto, K., H. Tanaka, I. Nagao, and Y. Ishizaka, 1997: Contribution of particulate sulfate and organic carbon to cloud condensation nuclei in the marine atmosphere. *Geophys. Res. Lett.,* **24,** 655–658.

Menon, S., and V. K. Saxena, 1998: Role of sulfates in regional cloud-climate interactions. *Atmos. Res.,* **47–48,** 299–315.

Monahan, E. C., D. E. Spiel, and K. L. Davidson, 1986: A model of marine aerosol generation via whitecaps and wave disruption. *Oceanic Whitecaps,* E. C. Monahan and G. Mac Niocaill, Eds., D. Reidel, 167–174.

Nakajima, T., and T. Nakajima, 1995: Wide-area determination of cloud microphysical properties from NOAA AVHRR measurements for FIRE and ASTEX regions. *J. Atmos. Sci.,* **52,** 4043–4059.

Novakov, T., C. Rivera-Carpio, J. E. Penner, and C. F. Rogers, 1994: The effect of anthropogenic sulfate aerosols on marine cloud droplet concentrations. *Tellus,* **46B,** 132–141.

O'Dowd, C. D., J. A. Lowe, and M. H. Smith, 1999: Coupling sea-salt and sulphate interactions and its impact on cloud droplet concentration predictions. *Geophys. Res. Lett.,* **26,** 1311–1314.

Penner, J. E., H. Eddleman, and T. Novakov, 1993: Towards the development of a global inventory of black carbon emissions. *Atmos. Environ.,* **27A,** 1277–1295.

Pincus, R., and M. B. Baker, 1994: Effect of precipitation on the albedo susceptibility of clouds in the marine boundary layer. *Nature,* **372,** 250–252.

——, and S. A. Klein, 2000: Unresolved spatial variability and microphysical process rates in large-scale models. *J. Geophys. Res.,* **105,** 27 059–27 065.

Platnick, S., and S. Twomey, 1994: Determining the susceptibility of cloud albedo to changes in droplet concentration with the Advanced Very High Resolution Radiometer. *J. Appl. Meteor.,* **33,** 334–347.

Putaud, J. P., and Coauthors, 2000: Chemical mass closure and assessment of the origin of the submicron aerosol in the marine boundary layer and the free troposphere at Tenerife during ACE-2. *Tellus.,* **52B,** 141–168.

Radke, L. F., J. A. Coakley, and M. D. King, 1989: Direct and remote sensing observations of the effects of ships on clouds. *Science,* **246,** 1146–1148.

Rasch, P. J., and J. E. Kristjánsson, 1998: A comparison of the CCM3 model climate using diagnosed and predicted condensate parameterization. *J. Climate,* **11,** 1587–1614.

Roelofs, G.-J., J. Lelieveld, and L. Ganzeveld, 1998: Simulation of global sulfate distribution and the influence on effective cloud drop radii with a coupled photochemistry-sulfur cycle model. *Tellus,* **50B,** 224–242.

Rosenfeld, D., 2000: Suppression of rain and snow by urban and industrial pollution. *Science,* **287,** 1793–1796.

Rosenzweig, C., and F. Abramopoulos, 1997: Land-surface model development for the GISS GCM. *J. Climate,* **10,** 2040–2054.

Rotstayn, L. D., 1999: Indirect forcing by anthropogenic aerosols: A global climate model calculation of the effective-radius and cloud-lifetime effects. *J. Geophys. Res.,* **104,** 9369–9380.

——, 2000: On the tuning of autoconversion parameterizations in climate models. *J. Geophys. Res.,* **105,** 15 495–15 507.

Saxena, V. K., and S. Menon, 1999: Sulfate-induced cooling in the southeastern U.S.: An observational assessment. *Geophys. Res. Lett.,* **26,** 2489–2492.

Snider, J. R., and J.-L. Brenguier, 2000: Cloud condensation nuclei and cloud droplet measurements during ACE-2. *Tellus,* **52B,** 828–842.

Spiro, P. A., D. J. Jacob, and J. A. Logan, 1992: Global inventory of sulfur emissions with a $1° \times 1°$ resolution. *J. Geophys. Res.,* **97,** 6023–6036.

Stowe, L. L., A. M. Ignatov, and R. R. Singh, 1997: Development, validation, and potential enhancements to the second-generation operational aerosol product at the National Environmental Satellite, Data, and Information Service of the National Oceanic and Atmospheric Administration. *J. Geophys. Res.,* **102,** 16 923–16 934.

Sundqvist, H., E. Berge, and J. E. Kristjansson, 1989: Condensation and cloud parameterization studies with a mesoscale numerical weather prediction model. *Mon. Wea. Rev.,* **117,** 1641–1657.

Taylor, J. P., and A. McHaffie, 1994: Measurement of cloud susceptibility. *J. Atmos. Sci.,* **51,** 1298–1306.

Tripoli, G. J., and W. R. Cotton, 1980: A numerical investigation of several factors contributing to the observed variable intensity of deep convection over south Florida. *J. Appl. Meteor.,* **19,** 1037–1063.

Twomey, S., 1977: The influence of pollution on the shortwave albedo of clouds. *J. Atmos. Sci.,* **34,** 1149–1152.

——, 1991: Aerosols, clouds and radiation. *Atmos. Environ.,* **25A,** 2435–2442.

Wang, J., W. B. Rossow, T. Uttal, and M. Rozendaal, 1999: Variability of cloud vertical structure during ASTEX observed from a combination of rawinsonde, radar, celiometer, and satellite. *Mon. Wea. Rev.,* **127,** 2482–2502.